Article

A Dual Channel Activatable Cyanine Dye for Mitochondrial Imaging and Mitochondria-Targeted Cancer Theranostics

Guang-Yu Pan, Hao-Ran Jia, Ya-Xuan Zhu, Ruo-Han Wang, Fu-Gen Wu, and Zhan Chen

ACS Biomater. Sci. Eng., **Just Accepted Manuscript** • DOI: 10.1021/acsbiomaterials.7b00480 • Publication Date (Web): 26 Sep 2017

A Dual Channel Activatable Cyanine Dye for Mitochondrial Imaging and Mitochondria-Targeted Cancer Theranostics

Guang-Yu Pan,[†,§] Hao-Ran Jia,[†,§] Ya-Xuan Zhu,[†] Ruo-Han Wang,[†] Fu-Gen Wu,*[,†] and Zhan Chen*[,‡]

[†]*State Key Laboratory of Bioelectronics, School of Biological Science and Medical Engineering, Southeast University, Nanjing 210096, P. R. China*

[‡]*Department of Chemistry, University of Michigan, 930 North University Avenue, Ann Arbor, Michigan 48109, United States*

KEYWORDS: *near-infrared heptamethine cyanine dye, turn-on response of visible light fluorescence, mitochondrial imaging/tracking, photothermal therapy, cell differentiation*

ABSTRACT

Since mitochondria are the key regulators for many cellular behaviors and are susceptible to hyperthermia and reactive oxygen species, mitochondria-specific reagents for simultaneous targeting, imaging, and treatment are highly desirable in cancer theranostics. Herein, we developed a mitochondria-targeted cyanine dye IR825-Cl which possesses two separated excitation wavelength channels for both red fluorescence imaging and near-infrared (NIR) photothermal therapy (PTT). For imaging, IR825-Cl could rapidly enter into cells and selectively target mitochondria. Although IR825-Cl was completely quenched in water, interestingly, this dye had a turn-on response of red fluorescence (610 nm) in mitochondria under 552 nm excitation due to its polarity-responsive fluorescence emission. More interestingly, IR825-Cl could realize the selective mitochondrial staining of cancer cells over normal cells, and could thus serve as an ideal fluorescent probe for identifying cancer cells in normal tissues, which will be extremely beneficial for cancer theranostics. For PTT, we demonstrated that under 808 nm NIR laser irradiation, this dye could efficiently convert optical energy into heat, realizing mitochondria-targeted photothermal cancer therapy. Collectively, this molecule realized both high fluorescence emission (QY > 43%) and effective light-to-heat conversion (17.4%), enabling its applications for wash-free fluorescence imaging for mitochondria and highly efficient fluorescence imaging-guided PTT.

1. INTRODUCTION

Mitochondria, the powerhouse of cells, are indispensable for energy production and cell survival. Besides, mitochondria are important regulators of many cellular behaviors, including cell apoptosis, calcium homeostasis, free radical production, and cell growth and differentiation.[1,2] Generally, mitochondrial dysfunctions are closely associated with several human diseases such as aging, neurodegenerative diseases, and cancer.[3] Therefore, maintaining a healthy population of mitochondria is essential for cell survival.[4] Mitochondrial imaging for probing the morphology and functions of mitochondria is crucial for evaluating the cellular state, and many fluorescent probes have been developed for the visualization and detection of mitochondria.[5–9] On the other hand, mitochondria are the key regulators of the intrinsic pathway of apoptosis,[1] which serves as a cell suicide program to eliminate cells in the organism.[10] Therefore, mitochondria-targeted therapeutic strategies hold great promise for cancer treatment due to their minimized toxic side effect, decreased multi-drug resistance, and improved therapeutic outcomes.[11] Photodynamic therapy (PDT), a form of phototherapy involving light and a photosensitizer, is used in conjunction with molecular oxygen to elicit cell death via the production of toxic radicals and reactive oxygen species (ROS).[12–16] Another important form of phototherapy is photothermal therapy (PTT), which utilizes heat generated from optical energy to cause thermal ablation of cancer cells with minimal invasiveness and high efficiency.[17–34] In particular, mitochondria-targeted PTT has attracted considerable interest because mitochondria are highly sensitive to hyperthermia[35] and ROS,[36] which may trigger mitochondrial ROS burst to cause apoptotic cell death.[37]

Previous studies have shown that by linking a mitochondrial targeting ligand, such as

triphenylphosphonium (TPP), and a fluorescent tag to the photothermal agent (PTA) can achieve simultaneous mitochondrial imaging and mitochondria-based PTT.[35,38] However, these strategies may confront with many practical problems, such as unsatisfied repeatability, toxicity concerns, and tedious chemical conjugation.[39] Besides, the conjugation of additional fluorescent tags may alter the pathway of the as-designed drugs (which may lead to compromised therapeutic efficacy) or lose the fluorescence tracking ability of the drugs once the fluorescent tags are released.[11] Therefore, it is imperative to develop a therapeutic agent with intrinsic fluorescence and mitochondrial targeting property.

Currently, lipophilic cationic heptamethine cyanine dyes have drawn much attention due to their mitochondrial targeting ability.[39–41] Many cyanine-based probes have been developed for the selective detection of mitochondrial ROS, glutathione, cysteine, pH, mitochondrial polarity, nitroreductase activity, and mitophagy.[4,42–49] Some cyanine-based molecules or composite materials possess a strong near-infrared (NIR) absorption character,[50–61] and they can realize not only phototherapy but also NIR fluorescence imaging under a single wavelength excitation.[62–72] However, effective PTT is always contradictory to fluorescence imaging in those systems, because a high fluorescence quantum yield (QY) usually compromises the photothermal conversion efficiency (η).[73]

Herein, we report a NIR heptamethine cyanine dye IR825-Cl with separated wavelength channels for simultaneous mitochondrial imaging as well as mitochondria-targeted PTT. As illustrated in Scheme 1, IR825-Cl with lipophilic indolium cation and benzyl group can rapidly enter into cells and selectively target mitochondria. Although IR825-Cl was completely quenched in water, interestingly, this dye had a turn-on response of red

fluorescence (610 nm) in mitochondria under 552 nm excitation. Besides, the cyanine dye with high NIR absorption also enabled effective PTT upon NIR (808 nm) laser irradiation. Collectively, the rationally designed IR825-Cl fundamentally addressed all the abovementioned paradox, making it an ideal agent in mitochondria-based imaging with strong fluorescence emission and highly efficient imaging-guided PTT.

Scheme 1. Schematic Illustration of Mitochondrial Imaging and Mitochondria-Targeted PTT of IR825-Cl.

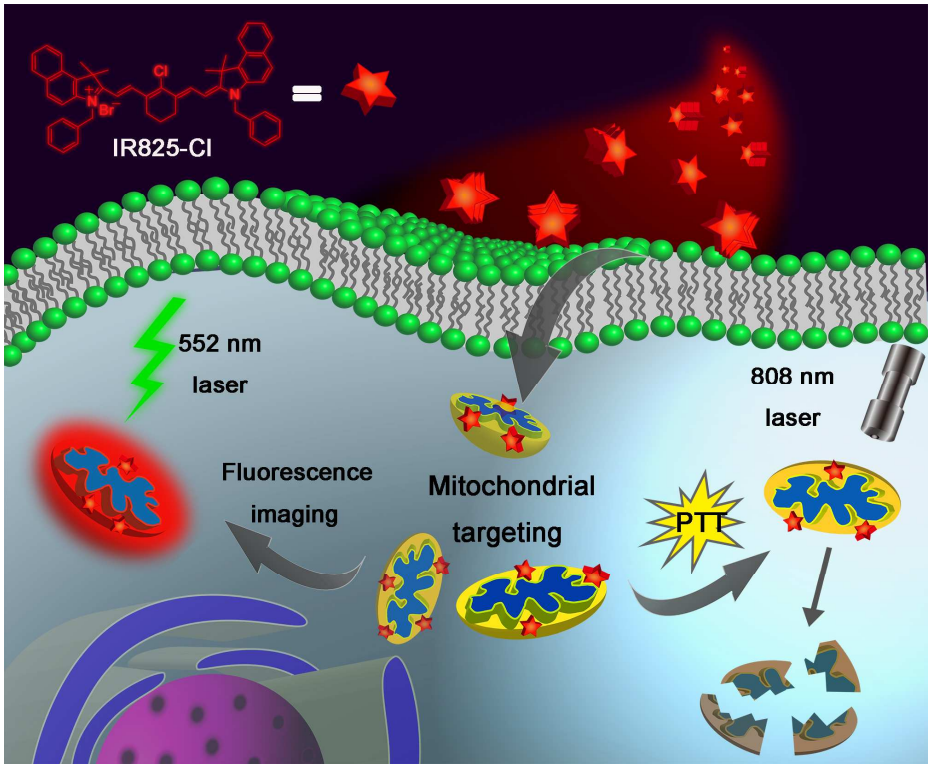

2. EXPERIMENTAL SECTION

2.1. Reagents and Materials. Unless stated otherwise, all chemicals and solvents were commercially obtained from commercial suppliers and used without further purification. 2,3,3-Trimethyl-4,5-benzo-3H-indole, benzyl bromide, and

3-(4,5-dimethyl-2-thiazolyl)-2,5-diphenyl-2-H-tetrazolium bromide (MTT) were obtained from Aladdin (China). Indocyanine green (ICG) and rhodamine 123 (Rhod 123) were purchased from Sigma Aldrich. Staurosporine (STS), calcein acetoxymethyl ester (calcein-AM), and propidium iodide (PI) were purchased from KeyGen Biotech. Inc., Nanjing, China. 1-Palmitoyl-2-oleoyl-sn-glycero-3-phosphocholine (POPC) and 1-palmitoyl-2-oleoyl-*sn*-glycero-3-phospho-(1'-*rac*-glycerol) (POPG) were ordered from Avanti Polar Lipids (USA). Deionized water (18.2 MΩ cm) was purified by a Milli-Q system (Millipore).

2.2. Synthesis and Characterization of IR825-Cl. As depicted in Figure 1a, compound 1[74] (7.60 g, 20 mmol, 2.0 eq), compound 2[75] (1.73 g, 10 mmol, 1.0 eq), and anhydrous sodium acetate (0.82 g, 10 mmol, 1.0 eq) were dissolved in acetic anhydride (250 mL), followed by stirring at 70 ^{o}C for 0.5 h under a N_2 atmosphere, resulting in a green solution. After completion of the reaction, the mixture was cooled to room temperature and dichloromethane (DCM) was then added, followed by being washed with a saturated aqueous solution of sodium bicarbonate. The organic extracts were dried over Na_2SO_4, filtered and evaporated. The crude product was purified by recrystallization from methanol-ether to produce compound 3 as a dark green solid. The as-synthesized product was characterized by ^{1}H NMR, ^{13}C NMR, and ESI-MS. ^{1}H NMR and ^{13}C NMR spectra were recorded on a Bruker Avance 300 MHz instrument. Mass spectra (MS) were measured with an Agilent 1260-6230 TOF LC-MS instrument. ^{1}H NMR (300 MHz, DMSO-d_6): δ 8.35 (t, J = 7.8 Hz, 4H), 8.07 (dd, J_1 = 8.7 Hz, J_2 = 7.8 Hz, 4H), 7.72 (dd, J_1 = 9.0 Hz, J_2 = 7.5 Hz, 4H), 7.54 (t, J = 7.8 Hz, 2H), 7.43 ~ 7.30 (m, 10H), 6.47 (d, J =14.4 Hz, 2H), 5.70 (s, 4H), 2.60 (t, J = 5.1 Hz, 4H), 2.01 (s, 12H), 1.80 (t, J = 5.4 Hz, 2H). ^{13}C NMR (75 MHz, DMSO-d_6): δ 174.0, 148.0, 142.4, 140.0, 135.0, 133.5, 131.5, 130.5, 129.9, 129.0, 127.8, 127.8, 127.5, 126.8, 126.5,

125.1, 122.3, 111.8, 101.8, 50.8, 47.3, 27.1, 25.7, 20.2. High-resolution MS (ESI): *m*/*z* calcd for $C_{52}H_{48}N_2Cl^+$ $[M - Br^-]^+$: 735.3506, found: 735.3550.

Absorption spectra were measured by a UV−vis spectrophotometer (UV-2600, Shimadzu, Japan) at the wavelength range of 300−900 nm. Fluorescence emission spectra of IR825-Cl excited by 552 and 580 nm were obtained by a spectrofluorophotometer (RF-5301PC, Shimadzu, Japan) and fluorescence emission spectra excited by 780 and 808 nm were collected with a fluorescence spectrometer (F-4600, Hitachi, Japan). IR825-Cl stock solution with a concentration of 10 mg/mL was prepared in DMSO and diluted with different solvents to a desired concentration prior to measurements.

The relative fluorescence quantum yield (QY) of IR825-Cl under 580 or 808 nm laser excitation was determined using rhodamine B in ethanol (QY = 0.970)[49] and ICG in methanol (QY = 0.043)[76] as the standard references and calculated using the following equation (1):[73]

$$QY_{\text{IR825-Cl}} = QY_{\text{S}} \times \frac{F_{\text{IR825-Cl}}}{F_{\text{S}}} \times \frac{A_{\text{S}}}{A_{\text{IR825-Cl}}} \qquad (1)$$

where $QY_{\text{IR825-Cl}}$ and QY_{S} are the relative quantum yields of IR825-Cl and the standard reference, respectively; $F_{\text{IR825-Cl}}$ and F_{S} are the integrated fluorescence intensities of IR825-Cl and the standard reference; $A_{\text{IR825-Cl}}$ and A_{S} are the absorption values of the two samples at the excitation wavelength.

2.3. Preparation of Neutral and Negatively Charged Liposomes. To prepare neutral liposomes, 4 mg of POPC was hydrated with 2 mL of phosphate-buffered saline (PBS) solution. Then, the lipid suspension was vortexed for 2 min and sonicated using a tip sonicator at 30 W with a 6 s-interval (4 s-pulse on, 2 s-pulse off) for a total of 2 min-pulse period. For negatively charged liposomes, typically, POPC and POPG powders were weighed separately with a molar ratio of 3 :

1 and dissolved in chloroform. The solution was evaporated under N_2 gas and completely vacuum-dried prior to use. Next, the POPC/POPG liposomes were prepared followed by the aforementioned procedure. To measure the hydrodynamic diameter and zeta potential of the as-prepared liposomes, 200 μg/mL liposomes in PBS solutions (pH = 7.4) were characterized by a Zetasizer (Nano ZS, Malvern, UK). For UV−vis absorption and fluorescence measurements, the liposome solutions were diluted with PBS solutions and mixed with an equal volume of 10 μg/mL IR825-Cl in PBS solutions to reach the final concentration of 10, 20, 50, 100, 200, 300, and 500 μg/mL. The mixed solutions were incubated for 30 min at room temperature before measurements. The fluorescence images of 5 μg/mL IR825-Cl in water and POPC/POPG solution (with a liposome concentration of 300 μg/mL) were imaged by a Cri Maestroin and PerkinElmer *in vivo* imaging system with excitation wavelength of 580 nm and emission wavelength of 620 nm.

2.4. Cell Culture. HeLa (human cervical cancer cell), A549 (lung cancer cell), HepG2 (liver cancer cell), MCF-7 (breast cancer cell), AT II (normal lung cell), or L02 (normal liver cell) cells were cultured in high-glucose complete Dulbecco's modified Eagle medium (DMEM) supplemented with 10% fetal bovine serum (FBS), 100 U/mL penicillin, and 100 μg/mL streptomycin. All the cells were incubated at 37 °C in a humidified incubator with 5% CO_2.

2.5. Subcellular Localization. To observe the subcellular localization of IR825-Cl, HeLa cells were first incubated with IR825-Cl (5.0 μg/mL) for 15 min, then, co-stained with Rhod 123 (10 μM) for 30 min before imaging under a confocal laser scanning microscope (TCS SP8, Leica, Germany) using a 63× objective lens. Rhod 123 was excited with a 488 nm laser and its fluorescence emission was collected at 500−550 nm and IR825-Cl was excited with a 552 nm laser and its fluorescence emission was collected at 580−660 nm. To observe the subcellular

localization of IR825-Cl in A549, HepG2, and MCF-7 cells, the same experimental procedures were conducted as described above. To observe the subcellular localization of IR825-Cl in AT II and L02 cells, cells were first incubated with IR825-Cl (5.0 μg/mL) for 6 h, and then co-stained with Rhod 123 (10 μM) for another 6 h. Finally, the confocal fluorescence images were taken immediately following the same procedures as described above.

2.6. Optimization of Staining Concentration. HeLa cells were first stained with 10 μM Rhod 123 for 30 min. After PBS washing, cells were stained with 0.5, 1.0, 2.0, 3.0, 4.0, 5.0, 6.0, 7.0, and 8.0 μg/mL IR825-Cl for 15 min, respectively. Finally, confocal fluorescence images were taken immediately.

2.7. Long-Term Confocal Imaging. HeLa cells were treated with 100 μL of culture medium containing 5.0 μg/mL IR825-Cl and placed into a cell incubator for different incubation time (1, 2, 3, 4, 6, 12, and 24 h). Before imaging, the treated cells were stained with 10 μM Rhod 123 for another 30 min. Then, the confocal fluorescence images were taken immediately with excitation at 488 and 552 nm and emission at 500−550 and 580−660 nm, respectively.

2.8. Confocal Imaging of HeLa Cells after Treatment with ICG. HeLa cells were treated with 100 μL of culture medium containing 5.0 μg/mL ICG and placed into a cell incubator for 30 min. Before imaging, the treated cells were washed by PBS for three times and stained with 10 μM Rhod 123 for 30 min. Then, the confocal fluorescence images were taken immediately with excitation at 488 and 633 nm and emission at 500−550 and 700−800 nm, respectively.

2.9. Isolation of Mitochondria from HeLa Cells. Mitochondria were isolated from cultured HeLa cells using a mitochondria isolation kit (Beyotime Institute of Biotechnology, Haimen, China). Briefly, the collected cell pellets (5×10^7 cells) were washed twice with cold PBS,

resuspended in mitochondria extraction solution (provided in the kit) and stirred in a homogenizer. Then, the obtained suspensions were centrifuged at 1000 g at 4 ^{o}C for 10 min and the supernatant was collected for further centrifugation at 11000 g at 4 ^{o}C for 10 min. The supernatant was discarded and the resultant precipitated mitochondria were collected. Next, the isolated mitochondria were incubated with 5.0 μg/mL IR825-Cl in a PBS solution at room temperature for 30 min before fluorescence measurements.

2.10. Evaluation on the Change of Mitochondrial Transmembrane Potential. HeLa cells were seeded into a 96-well confocal plate (5×10^3 cells per well) for 12 h. After PBS washing, HeLa cells were stained with 10 μM Rhod 123 and 5.0 μg/mL IR825-Cl for 30 min, respectively. Then, the treated cells were washed with PBS for three times and incubated with 100 μL of DMEM culture media containing 1 μM STS for 6 h. Finally, the confocal fluorescence images were acquired immediately with excitation at 488 and 552 nm and emission at 500−550 and 580−660 nm, respectively.

2.11. Confocal Imaging of Normal and Cancer Cells by IR825-Cl. For confocal imaging, A549 and AT II cells were stained with 5.0 μg/mL IR825-Cl for 30 min, respectively. Then the confocal fluorescence images were taken immediately with excitation at 552 nm and emission at 580−660 nm.

For confocal imaging of A549 and AT II cells co-cultured with different population ratios, the A549 and AT II cells with the ratios of 1 : 1, 1 : 5, and 1 : 10 were seeded in a 96-well confocal plate and incubated in a humidified incubator with 5% CO_2 for 24 h. After PBS washing, the cells were incubated with 100 μL of culture media containing 5.0 μg/mL of IR825-Cl for 30 min, and then the confocal images were taken immediately.

For confocal imaging of A549 and AT II cells co-cultured with the ratio of 1 : 1 at different incubation time pionts (1, 6, 12, and 24 h), 2.5×10^3 AT II cells and 2.5×10^3 A549 cells per well were seeded in a 96-well confocal plate and incubated in a humidified incubator with 5% CO_2 for 24 h, respectively. After PBS washing, the cells were incubated with 100 μL of culture media containing 5.0 μg/mL of IR825-Cl for different time periods (1, 6, 12, and 24 h), and then the confocal fluorescence images were taken immediately.

2.12. Photothermal Performance of IR825-Cl. The photothermal conversion efficiency (η) of IR825-Cl was evaluated according to a reported method.[77,78] Briefly, 300 μL of N_2-saturated water containing 20 μg/mL IR825-Cl or 20 μg/mL ICG was put in a 500 μL centrifuge tube and irradiated by a NIR laser (808 nm, 5.0 W/cm^2, total power 1.0 W) for 2 min. The laser was then switched off and the solution was cooled naturally. N_2-saturated pure water was used as a control group. An Ai50 NIR thermal imager was used to record the temperature changes.

The η of IR825-Cl and ICG was calculated using the following equations (2–5):

$$\eta = \frac{hS(T_{max} - T_{surr}) - Q_{dis}}{I(1 - 10^{-A_{808}})} \quad (2)$$

$$hS = \frac{\sum m_i C_i}{\tau_s} \quad (3)$$

$$\tau_s = -\frac{t}{\ln(\theta)} \quad (4)$$

$$\theta = \frac{T - T_{surr}}{T_{max} - T_{surr}} \quad (5)$$

In Eq. 2, h and S are the heat transfer coefficient and surface area of the container, respectively. T_{max} and T_{surr} are the final and initial temperature of the solution. Q_{dis} represents the heat dissipation of solvent, I is the laser power (typically I = 1.0 W) and A_{808} is the sample absorbance

at 808 nm. The A_{808} for IR825-Cl and ICG were 1.117 and 1.294, respectively. In Eq. 3, m and C are the mass (0.3 g) and heat capacity (4.2 J g^{-1} $^{o}C^{-1}$) of water. In Eq. 4, τ_s is time constant which was calculated by the linear fitting of t versus $-\ln(\theta)$. Wherein, t is the time after irradiation (Figure S14a) in unit of second (s). In Eq. 5, θ is the dimensionless driving force and T is the solution temperature. According to Figure S14, the ($T_{max} - T_{surr}$) for IR825-Cl and ICG was 28.7 and 27.5 ^{o}C, respectively; $\tau_{IR825\text{-}Cl}$ and τ_{ICG} were calculated to be 212 and 186 s, respectively. Therefore, the hS of IR825-Cl was 5.9 mW/^{o}C and that of ICG was 6.8 mW/^{o}C. The Q_{dis} of IR825-Cl and ICG were measured to be 9.49 and 10.84 mW, respectively. Substituting these parameters into the above equations, the η of IR825-Cl and ICG was calculated to be 17.4% and 18.5%, respectively.

2.13. Photothermal Evaluation of IR825-Cl. The photothermal properties of IR825-Cl was evaluated according to our previous work.[79] IR825-Cl solutions with different concentrations (0, 2, 5, 8, 10, 15, and 20 μg/mL) were placed in 500 μL centrifuge tubes and irradiated by an 808 nm NIR laser at 1.0 W/cm^2 for 5 min (beam spot 0.8 × 0.8 cm^2) at 25 ^{o}C, respectively. An Ai50 NIR thermal imager was used to record the temperature changes and acquire thermal images of the solution over time.

2.14. Cytotoxicity Evaluation of IR825-Cl and Its Photodegradation Products. The cytotoxicity of IR825-Cl against HeLa cells was determined by MTT assay. Typically, 5 × 10^3 HeLa cells per well were seeded in a 96-well plate and incubated for 24 h in a humidified incubator with 5% CO_2. Then the culture media were carefully aspired and cells were treated with 100 μL of culture media containing 0, 2, 5, 8, 10, 15, and 20 μg/mL of IR825-Cl, respectively, followed by incubation for another 24 h. Next, 10 μL of MTT solution (5.0 mg/mL in PBS) was

added to each well and incubated with the cells for 4 h. The formed formazan crystals were dissolved in 150 μL of DMSO. Following that, the plate was shaken for 10 min and the absorbance was measured at 570 nm on a microplate reader (Multiskan FC, Thermo-Scientific, USA). Each group was measured in triplicate. To evaluate the cytotoxicity of the photodegradation products of IR825-Cl, 1.0 mg/mL IR825-Cl solution was placed in centrifuge tubes and irradiated with an 808 nm NIR laser at 1.0 W/cm^2 for 2 h (beam spot 0.8 × 0.8 cm^2) to obtain completely photodegraded products. Then, MTT assay was carried out following the same procedure as described above.

2.15. In Vitro PTT. To evaluate the *in vitro* photothermal therapeutic effect of IR825-Cl, 5 × 10^3 HeLa cells per well were seeded in a 96-well plate and incubated for 24 h in a humidified incubator with 5% CO_2. Then cells were incubated with 100 μL of culture media with different concentrations (0, 2, 5, 8, 10, 15, and 20 μg/mL) of IR825-Cl for 4 h. After PBS washing, cells were exposed to 808 nm laser irradiation (1.0 W/cm^2) for 5 min in a 37 °C incubator. After another 24 h of incubation, the relative cell viabilities were determined by MTT assay as described above.

2.16. Flow Cytometric Analysis. To evaluate the cell death mechanism induced by IR825-Cl-mediated PTT, 2.5 × 10^4 HeLa cells per well were seeded in a 24-well plate and incubated for 24 h in a humidified incubator with 5% CO_2. Then, the cells were incubated with 500 μL of culture media containing different concentrations (0, 2, 5, or 10 μg/mL) of IR825-Cl for 4 h, respectively. After PBS washing, the cells were harvested and resuspended with 300 μL of serum-free culture media in 500 μL centrifuge tubes. Next, the cells were exposed to an 808 nm laser (1.0 W/cm^2) for 5 min in a 37 °C incubator, followed by centrifugation at 1000 rpm for 5 min. Afterward, the cells were treated with annexin V-fluorescein isothiocyanate (FITC)/PI

apoptosis detection kit (KeyGen Biotech. Inc., Nanjing, China) and analyzed using a flow cytometer (NovoCyte, ACEA Bioscience, SD).

To compare the *in vitro* photothermal therapeutic effect of ICG and IR825-Cl, the HeLa cells were incubated with 500 μL of culture media containing 20 μM ICG or 20 μM IR825-Cl, and then the flow cytometric experiments were carried out to analyze the apoptosis and necrosis ratios of the cells following the same procedure as described above.

2.17. Live/Dead Staining. 1×10^4 HeLa cells per well were seeded in a 96-well plate and incubated for 24 h in a humidified incubator with 5% CO_2. Cells were washed with PBS (pH 7.4) for three times and 100 μL of culture medium containing 10.0 μg/mL IR825-Cl was added to cells and incubated for another 4 h. Then, the cells were irradiated by an 808 nm NIR laser with different power densities (0, 0.3, 0.5, and 1.0 W/cm^2) for 10 min in a 37 °C incubator. Next, the cells were co-stained with 10 μM calcein-AM (*Ex*/*Em*: 495 nm/515 nm) and 10 μM PI (*Ex*/*Em*: 535 nm/617 nm) for 30 min in a 37 °C incubator, washed with PBS and finally imaged by a confocal microscope.

3. RESULTS AND DISCUSSION

3.1. Spectroscopic Properties of IR825-Cl in Solutions. IR825-Cl was successfully synthesized using the route outlined in Figure 1a and its chemical structure was characterized by ^{1}H nuclear magnetic resonance (NMR), ^{13}C NMR, and electrospray ionization mass spectrometry (ESI-MS) (Figure S1−3). We first studied the optical properties of IR825-Cl in water and various organic solvents. Generally, cyanine dyes exist as self-assembled aggregates in an aqueous solution via van der Waals forces and π−π stacking.[80] According to absorption spectroscopy, the aggregates

can be distinguished as H-aggregates with blue-shifted absorption (compared to monomers) or J-aggregates with red-shifted absorption.[81] As shown in Figure 1b, IR825-Cl in methanol exhibited strong NIR absorption at 824 nm, due to the monomeric form of IR825-Cl. However, its absorption band in water was broadened with a significantly blue-shifted peak at 745 nm, demonstrating that IR825-Cl mainly formed H-aggregates in water. Besides, the absorption spectra of IR825-Cl in different organic solvents (methanol, acetone, acetonitrile, ethanol, and chloroform) indicated that the maximum absorption of the molecule slightly shifted to a longer wavelength with the decrease of the solvent polarity (Table S1), implying its modest solvatochromism. Interestingly, although IR825-Cl emitted negligible fluorescence signal in water regardless of excitation wavelength, a new fluorescence band was observed in organic solvents under 580 nm excitation and the QY of IR825-Cl in ethanol was measured to be 43% (Figure 1c). Based on the absorption spectra, IR825-Cl molecules mainly exist as monomers in organic solvents. Therefore, the newly emerged fluorescence emission peak is assigned to monomeric IR825-Cl. The highly quenched fluorescence of IR825-Cl in water might be attributed to the formation of H-aggregates and the energy in excited state is dissipated elsewhere rather than through fluorescence emission. We also recorded the fluorescence spectra of IR825-Cl in NIR region under 808 nm excitation (Figure S4). However, whether in water or in methanol/ethanol, the fluorescence intensity of IR825-Cl was weak (QY < 0.14%). In comparison, ICG, a common NIR PTA, showed relatively high fluorescence intensity at 830 nm (QY = 4.3% in methanol).[76] Since it is known that an ideal PTA

should possess both high NIR absorption and low fluorescence QY to ensure the efficient conversion of optical energy into heat,[82] these results implied that IR825-Cl might serve as an excellent PTA.

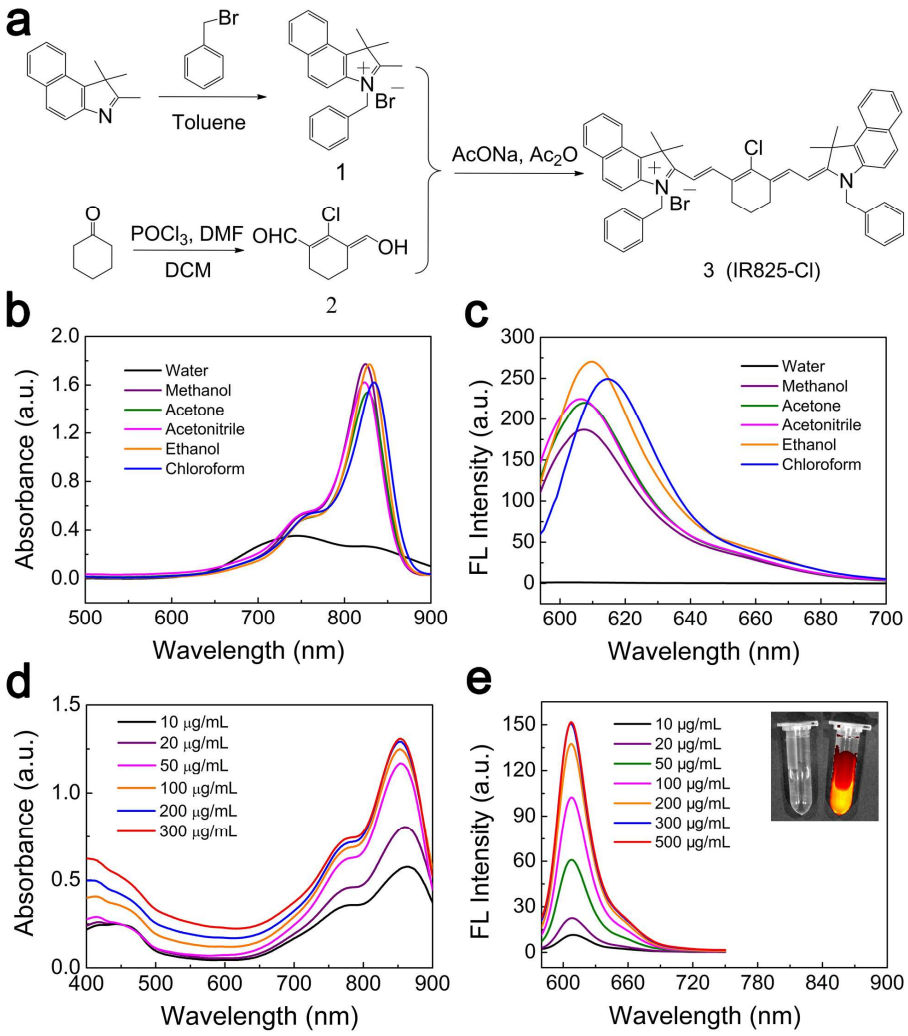

Figure 1. (a) Synthetic route of IR825-Cl. (b) UV–vis absorption spectra and (c) fluorescence spectra (*Ex*: 580 nm) of IR825-Cl (5 μg/mL) in different solvents. (d) UV–vis absorption spectra of IR825-Cl (5 μg/mL) in POPC/POPG solutions at different concentrations. (e) Fluorescence spectra of IR825-Cl (5 μg/mL) in POPC/POPG solutions at different liposome concentrations (*Ex*: 580 nm). Inset: Fluorescence images of IR825-Cl solutions (5 μg/mL; left: in water, right: in 300 μg/mL POPC/POPG solution) under 580 nm excitation.

Motivated by the fluorescence enhancement of IR825-Cl in organic solvents, we envisioned that it might achieve a turn-on fluorescence response upon hydrophobic anchoring into membranes. To this end, liposomes were adopted as model membranes to investigate the spectral behavior of IR825-Cl. We first prepared neutral liposomes composed of POPC with a diameter of 55.9 ± 18.7 nm and zeta potential of −0.3 mV in PBS (pH = 7.4). In a liposome solution, the absorption of IR825-Cl at 850 nm gradually rose with the increasing liposome concentration (Figure S5). This result implied the transformation from H-aggregates to monomers when IR825-Cl was inserted in the lipid hydrophobic tails. As expected, IR825-Cl showed gradually increased fluorescence intensities at 610 nm with the continuous addition of POPC liposomes (Figure S6). Considering that most biological membranes, such as plasma membrane and mitochondrial outer membrane, are negatively charged,[2] we prepared liposomes composed of POPC and the anionic lipid POPG at a molar ratio of 3 : 1, whose size and zeta potential were measured to be 56.1 ± 21.1 nm and –30 mV in PBS (pH = 7.4). The increase in the absorption and fluorescence of IR825-Cl molecules was also observed after their binding to the negatively charged POPC/POPG liposomes (Figure 1d,e). However, we noticed that negatively charged liposomes lead to stronger absorption of IR825-Cl. For example, 50 μg/mL POPC/POPG liposomes could induce a similar absorption increase of IR825-Cl to that of 500 μg/mL neutral liposomes (Figure 1d and S5). We also studied the spectral changes of IR825-Cl in POPC/POPG and POPC solutions in a time-dependent manner and found that the equilibrium time of the former (5 min) was much faster than that of the latter (30 min) (Figure S6 and S7). These results demonstrated that IR825-Cl, with a lipophilic cationic heptamethine core, could more efficiently bind to negatively charged

membranes via both electrostatic and hydrophobic interactions. Thus, we propose that the cyanine dye can bind to the negatively charged and hydrophobic mitochondrial membranes and achieve a turn-on response of visible light fluorescence.

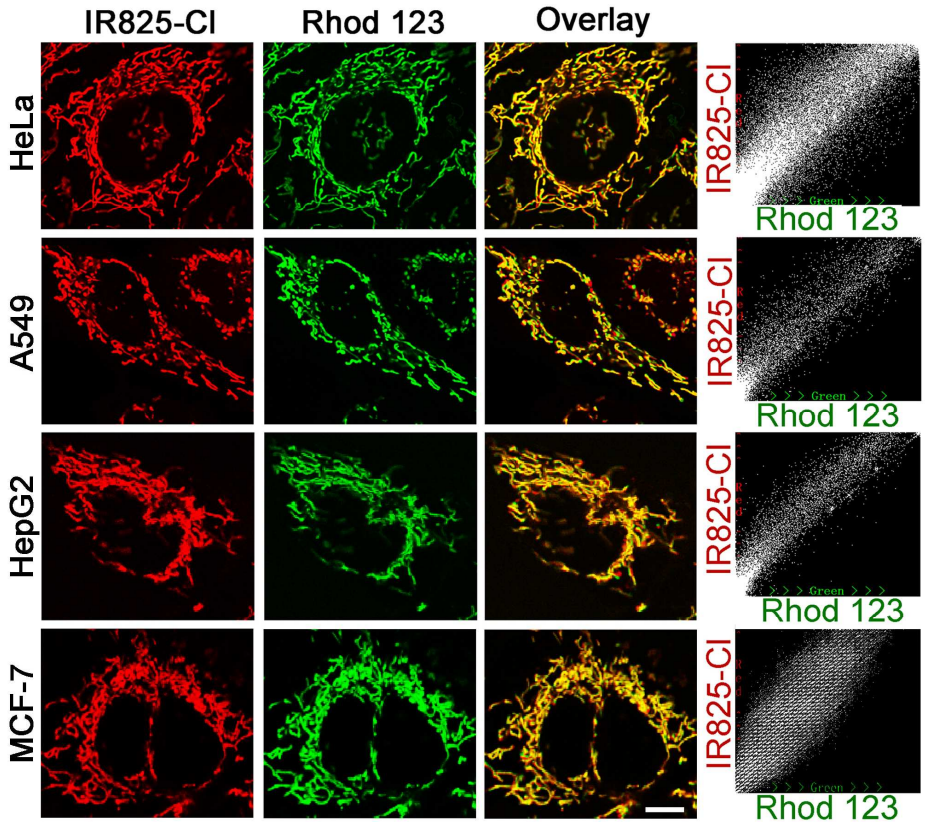

Figure 2. Confocal fluorescence images of HeLa, A549, HepG2, and MCF-7 cells co-stained with IR825-Cl and Rhod 123. Scale bar = 10 μm. Plots in the last column represent the intensity correlation plot of IR825-Cl and Rhod 123.

3.2. Selective Mitochondrial Imaging. One of the most distinguishing features of mitochondria is their large transmembrane potential (–180 mV) across mitochondrial inner membrane (negative inside).[2,83] Benefiting from this property, many lipophilic cations tend to accumulate in mitochondria rather than other organelles driven by the membrane potential gradient.[83] Therefore we expect that IR825-Cl may be suitable for mitochondrial targeting and may achieve responsive fluorescence imaging. To test our hypothesis, human cervical cancer

(HeLa) cells were co-stained with IR825-Cl and Rhod 123 (a commercial fluorescent probe of mitochondrion) and imaged under a confocal microscope. The red fluorescence signal distribution of IR825-Cl (*Ex*: 552 nm) completely merged with the green fluorescence signal of Rhod 123 (Figure 2). The Pearson's correlation coefficient (R_r) and overlap coefficient were 0.94 and 0.96, respectively, indicating the superior selectivity of the IR825-Cl probe for mitochondrial targeting. In addition, we optimized the imaging concentration of IR825-Cl (Figure S8) and found that 5 μg/mL IR825-Cl achieved satisfying wash-free mitochondrial imaging in a short time period (15 min) and could stably accumulate in mitochondria for at least 24 h without redistribution (Figure S9). Even after 48 h of PBS washing, IR825-Cl still enabled mitochondrial imaging with high quality (Figure S10). Besides, the cyanine dye could also label the mitochondria of other cancer cells (A549, R_r = 0.97; HepG2, R_r = 0.97; MCF-7, R_r = 0.90) (Figure 2), demonstrating their universal mitochondrial staining ability of cancer cells. To further prove the high affinity of IR825-Cl for mitochondria, the mitochondria of HeLa cells were isolated and incubated with IR825-Cl for fluorescence spectroscopic measurements. IR825-Cl in the mitochondrial suspension displayed a significantly enhanced emission peak at 610 nm (Figure 3), which was the same as that in liposome solutions. It has been reported that the mitochondrial localization of lipophilic cations is usually transmembrane potential ($\Delta\Psi$m)-dependent. To investigate the influence of $\Delta\Psi$m on the mitochondrial accumulation of IR825-Cl, HeLa cells were treated with both IR825-Cl and Rhod 123 (which is also a $\Delta\Psi$m indicator), followed by the treatment of 1 μM STS to disrupt the $\Delta\Psi$m. As shown in Figure S11, neither IR825-Cl nor Rhod 123 could stain the mitochondria after 6 h of STS treatment, demonstrating that the mitochondrial targeting

ability of IR825-Cl was also $\Delta\Psi$m-dependent.

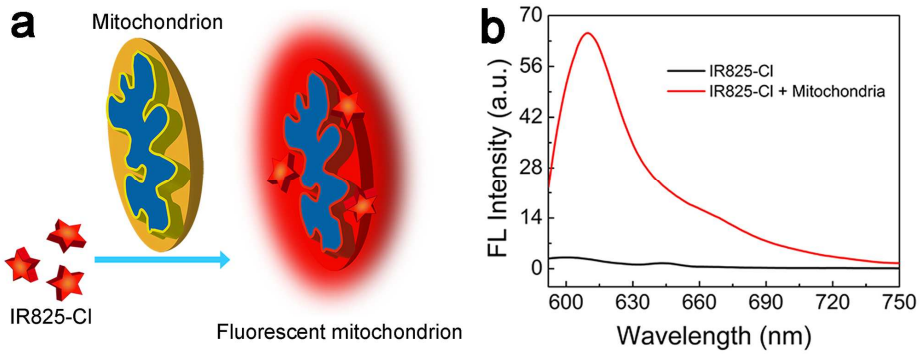

Figure 3. (a) Schematic illustration of the fluorescence staining of isolated mitocondrion by IR825-Cl. (b) Fluorescence emission spectra (*Ex* = 580 nm) of IR825-Cl (5.0 μg/mL) in water and in isolated mitochondrial suspension, respectively.

3.3. Preferred Mitochondrial Staining of Cancer Cells over Normal Cells by IR825-Cl.

It is known that the mitochondrial membrane potential (MMP) of cancer cells is usually more negative than that of normal cells,[11] with a difference of at least 60 mV.[84,85] In addition, cancer cells need more nutrition than normal cells. Therefore, cancer cells will internalize more IR825-Cl molecules than normal cells for the stronger electrostatic interaction between IR825-Cl and the mitochondria of cancer cells, resulting in the stronger fluorescence of mitochondria in cancer cells. To test our hypothesis, normal lung cells (AT II) and cancerous lung cells (A549) were stained with IR825-Cl and imaged under a confocal microscope (Figure 4). Under the same incubation and imaging conditions, the mitochondria in A549 cells with strong red fluorescence were clearly observed; however, very weak fluorescence could be seen in AT II cells. Thus, the confocal fluorescence images of the A549 and AT II cells confirmed the preferred interaction between IR825-Cl and cancer cells.

To confirm if IR825-Cl can also differentiate cancer cells from normal cells in a real

tumor-mimic environment, the cancerous A549 cells and the normal AT II cells were mixed with the ratios of 1 : 1, 1 : 5, and 1 : 10, respectively, and the cell mixtures were co-cultured in a 96-well confocal plate and then incubated with IR825-Cl. As showed in Figure 5, the fluorescence of A549 cells is in sharp contrast with that of AT II cells in all the cell mixtures. In addition, such a sharp fluorescence difference between the two cells did not alter within a time period of 24 h (Figure S12). The above results demonstrated that IR825-Cl was an ideal fluorescent probe for identifying cancer cells in normal tissues.

We need to mention that although the fluorescence emission of the mitochondria in normal cells such as AT II and L02 stained by IR825-Cl was relatively low at a short incubation time period (e.g., 30 min), the staining performance was significantly improved when the incubation time was extended to 6 h with the R_r of AT II and L02 reaching 0.95 and 0.96, respectively (Figure S13), suggesting that the IR825-Cl could also achieve satisfying mitochondrial staining of normal cells at elevated incubation time.

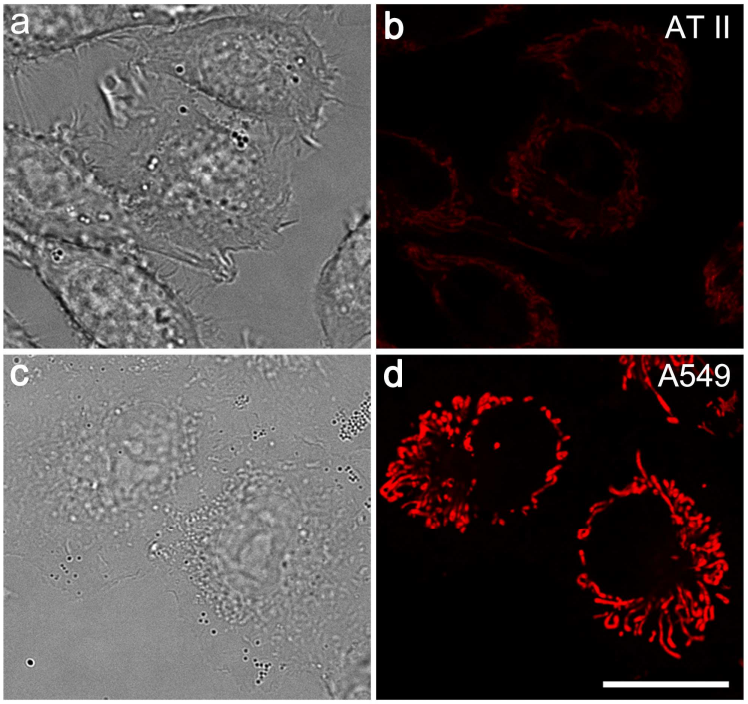

Figure 4. Differentiation between cancerous A549 cells and normal AT II cells by IR825-Cl. (a) Bright-field and (b) fluorescence images of IR825-Cl-treated AT II cells. (c) Bright-field and (d) fluorescence images of IR825-Cl-treated A549 cells. Scale bar = 20 μm. Before imaging, A549 and AT II cells were incubated with IR825-Cl (5.0 μg/mL) for 30 min.

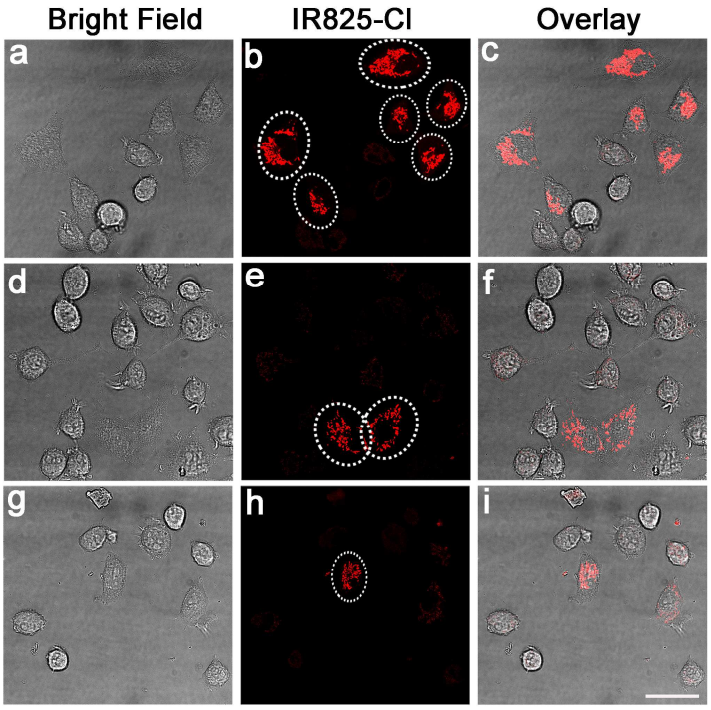

Figure 5. Confocal images of the mixed A549 and AT II cells with the A549/AT II ratios of (a–c) 1 : 1, (d–f) 1 : 5, and (g–i) 1 : 10. The dotted circles indicate the presence of A549 cells.

3.4. Photothermal Properties of IR825-Cl. Based on the high NIR absorption and the superior mitochondrial targeting property of IR825-Cl, we believe that IR825-Cl will be effective for mitochondria-based PTT. To test this, we first measured the η of IR825-Cl according to a previously reported method.[77,78] The η of IR825-Cl was calculated to be 17.4%, which is comparable to that of ICG (18.5%) (Figure S14). We then measured the temperature changes of IR825-Cl solutions at different concentrations upon laser irradiation, and a concentration-dependent temperature increase upon laser irradiation was observed (Figure 6a). Particularly, the temperature of 20 μg/mL IR825-Cl solution was found to increase sharply (~17 ^{o}C), while the temperature only increased slightly (~2 ^{o}C) in a PBS solution. These results confirmed that IR825-Cl is also an eligible PTA.

3.5. *In Vitro* PTT. Subsequently, *in vitro* PTT and dark cytotoxicity evaluation of IR825-Cl

were conducted for HeLa cells. In the PTT group, the cells were first incubated with different concentrations of IR825-Cl for 4 h and then irradiated by an 808 nm laser (1.0 W/cm^2) for 5 min. The results revealed a decreasing trend of cell viability with the increasing concentration of IR825-Cl. Particularly, only 5 μg/mL IR825-Cl could kill approximately 70% cancer cells during PTT and > 95% cell death was observed at higher concentrations of the agent. In the non-irradiation group, IR825-Cl showed low cytotoxicity at the concentrations below 20 μg/mL (Figure 6b). We also studied the cell death mechanism induced by IR825-Cl-mediated PTT by using flow cytometry (Figure 7), and it was found that the combined treatment of 10 μg/mL IR825-Cl and laser irradiation induced the death of HeLa cells mainly through late apoptosis/necrosis (80.15%). To intuitively confirm the phototoxicity of IR825-Cl, PTT-treated HeLa cells were co-stained with calcein-AM (to stain live cells green) and PI (to stain dead cells red) (Figure 8a). The results verified that IR825-Cl exhibited excellent anticancer performance upon NIR laser irradiation. It has been reported that the mitochondria of cancer cells are highly sensitive to heat shock and only a mild temperature elevation of mitochondria could induce apoptotic cell death.[35]

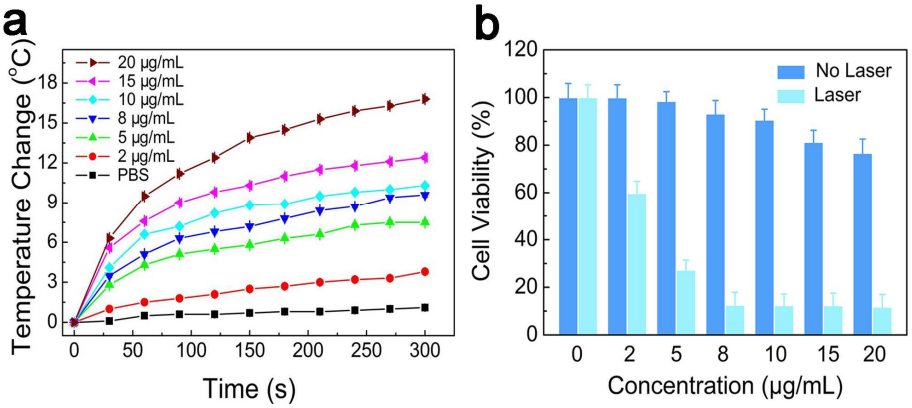

Figure 6. (a) Temperature changes of different concentrations of IR825-Cl in PBS solutions upon irradiation by an 808 nm laser (1.0 W/cm^2) for 5 min. (b) Relative viability of

IR825-Cl-treated HeLa cells with or without laser irradiation.

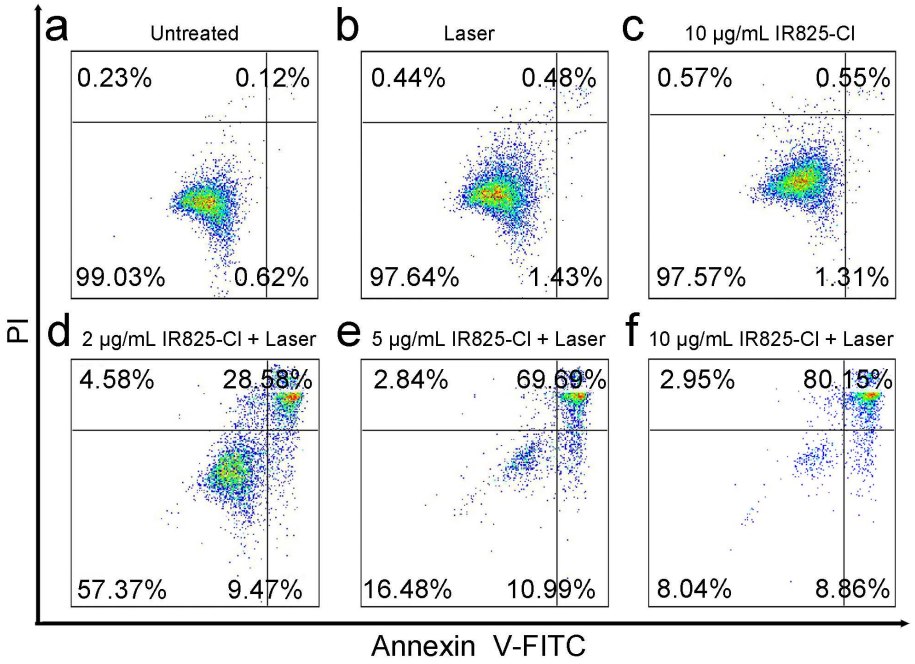

Figure 7. Flow cytometric analyses of the annexin V-FITC/PI staining results of HeLa cells after different treatments as indicated.

To highlight the advantages of mitochondrial targeting for photothermal therapy, ICG, a U.S. Food and Drug Administration (FDA) approved dye for routine clinical use, was selected for comparison. Although the η of IR825-Cl and ICG was almost equal, the PTT outcome of IR825-Cl was much better than that of ICG (Figure S15), which did not accumulate in mitochondria (Figure S16). Thus, apart from the high η of IR825-Cl, its mitochondrial targeting ability also contributed to the excellent PTT performance. It is worth noting that IR825-Cl as an organic cyanine dye can degrade into smaller molecules upon NIR laser irradiation,[86] we therefore evaluated the cytotoxicity of these photodegradation products towards normal cells. The results demonstrated that the degraded products possessed negligible cytotoxicity to L02 cells even at a high concentration of 80 μg/mL (Figure 8b),

suggesting the little toxic side effect of IR825-Cl during the in vivo PTT treatment. Therefore, as an ideal mitochondrial imaging agent with turn-on response of visible-light fluorescence as well as an excellent photothermal agent with few side effects and efficient phototherapeutic outcome, IR825-Cl meets all the requirements of cancer theranostics.

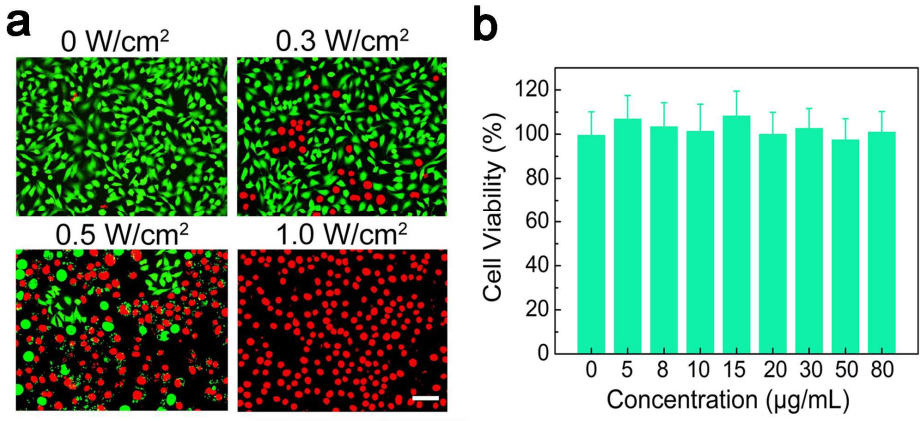

Figure 8. (a) Confocal fluorescence images of HeLa cells co-stained by calcein-AM and PI after PTT treatments with different irradiation doses indicated. (b) Relative viability of L02 cells after incubation with various concentrations of photodegradation products of IR825-Cl for 24 h.

3.6. Advantages of the Two Separated Excitation Channels of IR825-Cl. As depicted in Figure 9, for conventional NIR PTAs (e.g., ICG) with a single excitation wavelength, the energy of excited state is dissipated either by internal conversion (vibration as heat) or fluorescence emission.[87] Therefore, these two pathways are antagonistic to each other. Whereas, IR825-Cl possesses two separated excitation channels: when excited by 552 nm, the energy is dominantly dissipated through the emission of fluorescence; at the excitation of 808 nm, thermal decay is the main pathway of energy release. Hence, this cyanine dye achieved both high-quality fluorescence imaging and efficient photothermal conversion.

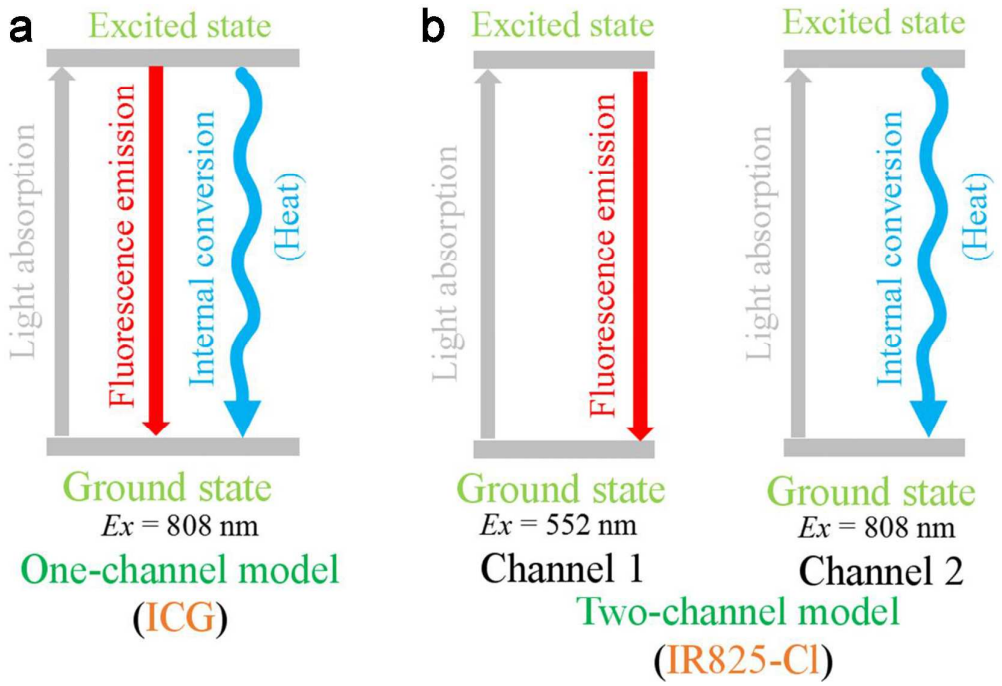

Figure 9. Schematic illustration of the photophysical processes for (a) the one-channel model (such as for ICG) and (b) the two-channel model (such as for IR825-Cl).

4. CONCLUSION

In summary, we have rationally designed a dual-functional cyanine dye IR825-Cl with separated wavelength channels for simultaneous mitochondrial fluorescence imaging and mitochondria-targeted PTT. Although IR825-Cl was completely quenched in aqueous solutions, it presented a turn-on fluorescence response at ~610 nm with a high QY (> 43%) in organic solvents or in a less polar membrane environment. Benefiting from its lipophilic cationic property[39–41] and the help of benzyl groups,[49] IR825-Cl could rapidly enter into cells and selectively accumulate in mitochondria, which achieved wash-free red fluorescence imaging for mitochondria due to its polarity-responsive fluorescence enhancement property. Since NIR fluorescent probes are restricted either by their relatively low QY or the lack of

commercial NIR fluorescence microscopes, the development of red fluorescent mitochondrial probe of IR825-Cl can readily find numerous applications in mitochondria-related cell biology. In addition, IR825-Cl could differentiate cancer cells from normal cells, which ensures its application as an excellent cancer diagnostic reagent. More importantly, IR825-Cl possesses high NIR absorption and low fluorescence QY (~0.14%) at the excitation of 808 nm, which ensure its high η (17.4%). Therefore, IR825-Cl can serve as an effective mitochondria-targeted PTA and achieve markedly enhanced anticancer efficacy since mitochondrion as a critical cellular organelle for cell survival is highly sensitive to hyperthermia. Taken together, benefiting from its two channel mechanism, IR825-Cl can realize bright fluorescence imaging without the sacrifice of its photothermal conversion efficiency. Moreover, not only IR825-Cl but also its photodegradation products have low cytotoxicity. We believe that IR825-Cl as a small and dual functional organic molecule with good biocompatibility will find wide applications in theranostics.

ASSOCIATED CONTENT

Supporting Information

The Supporting Information is available free of charge on the ACS Publications website at DOI:

Figures S1−S16, Table S1 (PDF)

AUTHOR INFORMATION

Corresponding Authors

*(F.G.W.) E-mail: wufg@seu.edu.cn.

*(Z.C.) E-mail: zhanc@umich.edu.

Author Contributions

§G.Y.P. and H.R.J. contributed equally.

Notes

The authors declare no competing financial interest.

ACKNOWLEDGMENTS

This work was supported by grants from the National High-tech R&D Program of China (863 Program) (2015AA020502), National Natural Science Foundation of China (21673037), Natural Science Foundation of Jiangsu Province (BK20170078), Fundamental Research Funds for the Central Universities, and Six Talents Peak Project in Jiangsu Province (2015-SWYY-003). ZC acknowledges the support from the University of Michigan.

REFERENCES

(1) Fulda, S.; Galluzzi, L.; Kroemer, G. Targeting Mitochondria for Cancer Therapy. *Nat. Rev. Drug Discov*. **2010**, *9*, 447–464.

(2) Jean, S. R.; Ahmed, M.; Lei, E. K.; Wisnovsky, S. P.; Kelley, S. O. Peptide-Mediated Delivery of Chemical Probes and Therapeutics to Mitochondria. *Acc. Chem. Res.* **2016**, *49*, 1893–1902.

(3) Wallace, D. C. A Mitochondrial Paradigm of Metabolic and Degenerative Diseases, Aging, and Cancer: a Dawn for Evolutionary Medicine. *Annu. Rev. Genet.* **2005**, *39*, 359–407.

(4) Liu, Y.; Zhou, J.; Wang, L. L.; Hu, X. X.; Liu, X. J.; Liu, M. R.; Cao, Z. H.; Shangguan, D. H.; Tan, W. H. A Cyanine Dye to Probe Mitophagy: Simultaneous Detection of Mitochondria and Autolysosomes in Live Cells. *J. Am. Chem. Soc.* **2016**, *138*, 12368–12374.

(5) Zhu, H.; Fan, J. L.; Du, J. J.; Peng, X. J. Fluorescent Probes for Sensing and Imaging within Specific Cellular Organelles. *Acc. Chem. Res*. **2016**, *49*, 2115–2126.

(6) Leung, C. W. T.; Hong, Y. N.; Chen, S. J.; Zhao, E. G.; Lam, J. W. Y.; Tang, B. Z. A Photostable

AIE Luminogen for Specific Mitochondrial Imaging and Tracking. *J. Am. Chem. Soc.* **2013**, *135*, 62–65.

(7) Zhou, F. F.; Xing, D.; Wu, B. Y.; Wu, S. N.; Ou, Z. M.; Chen, W. R. New Insights of Transmembranal Mechanism and Subcellular Localization of Noncovalently Modified Single-Walled Carbon Nanotubes. *Nano Lett.* **2010**, *10*, 1677–1681.

(8) Kaloyanova, S.; Zagranyarski, Y.; Ritz, S.; Hanulová, M.; Koynov, K.; Vonderheit, A.; Müllen, K.; Peneva, K. Water-Soluble NIR-Absorbing Rylene Chromophores for Selective Staining of Cellular Organelles. *J. Am. Chem. Soc.* **2016**, *138*, 2881–2884.

(9) Gu, X. G.; Zhao, E. G.; Zhao, T.; Kang, M. M.; Gui, C.; Lam, J. W. Y.; Du, S. W.; Loy, M. M. T.; Tang, B. Z. A Mitochondrion-Specific Photoactivatable Fluorescence Turn-On AIE-Based Bioprobe for Localization Super-Resolution Microscope. *Adv. Mater.* **2016**, *28*, 5064–5071.

(10) Ashkenazi, A.; Herbst, R. S. To kill a Tumor Cell: the Potential of Proapoptotic Receptor Agonists. *J. Clin. Invest.* **2008**, *118*, 1979–1990.

(11) Hu, Q. L.; Gao, M.; Feng, G. X.; Liu, B. Mitochondria-Targeted Cancer Therapy Using a Light-Up Probe with Aggregation-Induced-Emission Characteristics. *Angew. Chem., Int. Ed.* **2014**, *53*, 14225–14229.

(12) Lovell, J. F.; Liu, T. W. B.; Chen, J.; Zheng, G. Activatable Photosensitizers for Imaging and Therapy. *Chem. Rev.* **2010**, *110*, 2839–2857.

(13) Zhang, M.; Zhang, Z. H.; Blessington, D.; Li, H.; Busch, T. M.; Madrak, V.; Miles, J.; Chance, B.; Glickson, J. D.; Zheng, G. Pyropheophorbide 2-Deoxyglucosamide: A New Photosensitizer Targeting Glucose Transporters. *Bioconjugate Chem.* **2003**, *14*, 709–714.

(14) Chen, J.; Stefflova, K.; Niedre, M. J.; Wilson, B. C.; Chance, B.; Glickson, J. D.; Zheng, G. Protease-Triggered Photosensitizing Beacon Based on Singlet Oxygen Quenching and Activation. *J. Am. Chem. Soc.* **2004**, *126*, 11450–11451.

(15) Stefflova, K.; Chen, J.; Marotta, D.; Li, H.; Zheng, G. Photodynamic Therapy Agent with a Built-In Apoptosis Sensor for Evaluating Its Own Therapeutic Outcome in Situ. *J. Med. Chem.* **2006**, *49*, 3850–3856.

(16) Stefflova, K., Li, H., Chen, J.; Zheng, G. Peptide-Based Pharmacomodulation of a Cancer-Targeted Optical Imaging and Photodynamic Therapy Agent. *Bioconjugate Chem.* **2007**, *18*, 379–388.

(17) O'Neal, D. P.; Hirsch, L. R.; Halas, N. J.; Payne, J. D.; West, J. L. Photo-Thermal Tumor Ablation in Mice Using Near Infrared-Absorbing Nanoparticles. *Cancer Lett.* **2004**, *209*, 171–176.

(18) Huang, X. H.; El-Sayed, I. H.; Qian, W.; El-Sayed, M. A. Cancer Cell Imaging and Photothermal Therapy in the Near-Infrared Region by Using Gold Nanorods. *J. Am. Chem. Soc.* **2006**, *128*, 2115–2120.

(19) Lovell, J. F.; Jin, C. S., Huynh, E.; Jin, H. L.; Kim, C.; Rubinstein, J. L.; Chan, W. C. W.; Cao, W. G.; Wang, L. V.; Zheng, G. Porphysome Nanovesicles Generated by Porphyrin Bilayers for

Use as Multimodal Biophotonic Contrast Agents. *Nat*. *Mater*. **2011**, *10*, 324−332.

(20) Zeng, C. T.; Shang, W. T.; Liang, X. Y.; Liang, X.; Chen, Q. S.; Chi, C. W.; Du,; Y. Fang, C. H.; Tian, J. Cancer Diagnosis and Imaging-Guided Photothermal Therapy Using a Dual-Modality Nanoparticle. *ACS Appl*. *Mater*. *Interfaces* **2016**, *8*, 29232–29241.

(21) Wang, L.; Gao, C.; Liu, K. Y.; Liu, Y. X.; Ma, L. Y.; Liu, L. D.; Du, X. X.; Zhou, J. Cypate-Conjugated Porous Upconversion Nanocomposites for Programmed Delivery of Heat Shock Protein 70 Small Interfering RNA for Gene Silencing and Photothermal Ablation. *Adv*. *Funct*. *Mater*. **2016**, *26*, 3480–3489.

(22) Chen, Y. J.; Li, Z. H.; Wang, H. B.; Wang, Y.; Han, H. J.; Jin, Q.; Ji, J. IR-780 Loaded Phospholipid Mimicking Homopolymeric Micelles for Near-IR Imaging and Photothermal Therapy of Pancreatic Cancer. *ACS Appl*. *Mater*. *Interfaces* **2016**, *8*, 6852–6858.

(23) Zheng, M.; Li,Y.; Liu, S.; Wang, W. Q.; Xie, Z. G.; Jing, X. B. One-Pot to Synthesize Multifunctional Carbon Dots for Near Infrared Fluorescence Imaging and Photothermal Cancer Therapy. *ACS Appl*. *Mater*. *Interfaces* **2016**, *8*, 23533–23541.

(24) Zhang, Y. Y.; Teh, C.; Li, M. H.; Ang, C. Y.; Tan, S. Y.; Qu, Q. Y.; Korzh, V.; Zhao, Y. L. Acid-Responsive Polymeric Doxorubicin Prodrug Nanoparticles Encapsulating a Near-Infrared Dye for Combined Photothermal-Chemotherapy. *Chem*. *Mater*. **2016**, *28*, 7039–7050.

(25) Yang, Y.; Liu, J. J.; Liang, C.; Feng, L. Z.; Fu, T. T.; Dong, Z. L.; Chao, Y.; Li, Y. G.; Lu, G.; Chen, M. W.; Liu, Z. Nanoscale Metal–Organic Particles with Rapid Clearance for Magnetic Resonance Imaging-Guided Photothermal Therapy. *ACS Nano* **2016**, *10*, 2774–2781.

(26) Kim, S. H.; Lee, J. E.; Sharker, S. M.; Jeong, J. H.; In, I.; Park, S. Y. In Vitro and in Vivo Tumor Targeted Photothermal Cancer Therapy Using Functionalized Graphene Nanoparticles. *Biomacromolecules* **2015**, *16*, 3519–3529.

(26) Huang, P.; Rong, P. F.; Jin, A.; Yan, X. F.; Zhang, M. G.; Lin, J.; Hu, H.; Wang, Z.; Yue, X. L.; Li, W. W.; Niu, G.; Zeng, W. B.; Wang, F.; Zhou, K. C.; Chen, X. Y. Dye-Loaded Ferritin Nanocages for Multimodal Imaging and Photothermal Therapy. *Adv*. *Mater*. **2014**, *26*, 6401–6408.

(28) Wang, J.; Zhu, G. Z.; You, M. X.; Song, E. Q.; Shukoor, M. I.; Zhang, K. J.; Altman, M. B.; Chen, Y.; Zhu, Z.; Huang, C. Z.; Tan, W. H. Assembly of Aptamer Switch Probes and Photosensitizer on Gold Nanorods for Targeted Photothermal and Photodynamic Cancer Therapy. *ACS Nano* **2012**, *6*, 5070–5077.

(29) Wang, N. N.; Zhao, Z. L.; Lv, Y. F.; Fan, H. H.; Bai, H. R.; Meng, H. M.; Long, Y. Q.; Fu, T.; Zhang, X. B.; Tan, W. H. Gold Nanorod-Photosensitizer Conjugate with Extracellular pH-Driven Tumor Targeting Ability for Photothermal/Photodynamic Therapy. *Nano Res*. **2014**, *7*, 1291–1301.

(30) Liang, X. L.; Li, Y. Y.; Li, X. D.; Jing, L. J.; Deng, Z. J.; Yue, X. L.; Li, C. H.; Dai, Z. F. PEGylated Polypyrrole Nanoparticles Conjugating Gadolinium Chelates for Dual-Modal MRI/Photoacoustic Imaging Guided Photothermal Therapy of Cancer. *Adv*. *Funct*. *Mater*. **2015**,

25, 1451–1462.

(31) Zha, Z. B.; Yue, X. L.; Ren, Q. S.; Dai, Z. F. Uniform Polypyrrole Nanoparticles with High Photothermal Conversion Efficiency for Photothermal Ablation of Cancer Cells. *Adv. Mater.* **2013**, *25*, 777–782.

(32) Chen, M.; Tang, S. H.; Guo, Z. D.; Wang, X. Y.; Mo, S. G.; Huang, X. Q.; Liu, G.; Zheng, N. F. Core–Shell Pd@ Au Nanoplates as Theranostic Agents for in-Vivo Photoacoustic Imaging, CT Imaging, and Photothermal Therapy. *Adv. Mater.* **2014**, *26*, 8210–8216.

(33) Lin, L. S.; Cong, Z. X.; Cao, J. B.; Ke, K. M.; Peng, Q. L.; Gao, J. H.; Yang, H. H.; Liu, G.; Chen, X. Y. Multifunctional Fe_3O_4@Polydopamine Core–Shell Nanocomposites for Intracellular mRNA Detection and Imaging-Guided Photothermal Therapy. *ACS Nano* **2014**, *8*, 3876–3883.

(34) Zheng, T. T.; Li, G. G.; Zhou, F.; Wu, R.; Zhu, J. J.; Wang, H. Gold-Nanosponge-Based Multistimuli-Responsive Drug Vehicles for Targeted Chemo-Photothermal Therapy. *Adv. Mater.* **2016**, *28*, 8218–8226.

(35) Jung, H. S.; Han, J. Y.; Lee, J. H.; Lee, J. H.; Choi, J. M.; Kweon, H. S.; Han, J. H.; Kim, J. H.; Byun, K. M.; Jung, J. H.; Kang, C. H.; Kim, J. S. Enhanced NIR Radiation-Triggered Hyperthermia by Mitochondrial Targeting. *J. Am. Chem. Soc.* **2015**, *137*, 3017–3023.

(36) Yu, C. Y. Y.; Xu, H.; Ji, S. L.; Kwok, R. T. K.; Lam, J. W. Y.; Li, X. L.; Krishnan, S.; Ding, D.; Tang, B. Z. Mitochondrion-Anchoring Photosensitizer with Aggregation-Induced Emission Characteristics Synergistically Boosts the Radiosensitivity of Cancer Cells to Ionizing Radiation. *Adv. Mater.* **2017**, *29*, 1606167.

(37) Yu, Z. Z.; Sun, Q. Q.; Pan, W.; Li, N.; Tang, B. A Near-Infrared Triggered Nanophotosensitizer Inducing Domino Effect on Mitochondrial Reactive Oxygen Species Burst for Cancer Therapy. *ACS Nano* **2015**, *9*, 11064–11074.

(38) Chen, S.; Lei, Q.; Qiu, W. X.; Liu, L. H.; Zheng, D. W.; Fan, J. X.; Rong, L.; Sun, Y. X.; Zhang, X. Z. Mitochondria-Targeting "Nanoheater" for Enhanced Photothermal/Chemo-Therapy. *Biomaterials* **2017**, *117*, 92–104.

(39) Luo, S. L.; Tan, X.; Fang, S. T.; Wang, Y.; Liu, T.; Wang, X.; Yuan, Y.; Sun, H. Q.; Qi, Q. R.; Shi, C. M. Mitochondria-Targeted Small-Molecule Fluorophores for Dual Modal Cancer Phototherapy. *Adv. Funct. Mater.* **2016**, *26*, 2826–2835.

(40) Wang, Y.; Liu, T.; Zhang, E. L.; Luo, S. L.; Tan, X.; Shi, C. M. Preferential Accumulation of the Near Infrared Heptamethine Dye IR-780 in the Mitochondria of Drug-Resistant Lung Cancer Cells. *Biomaterials* **2014**, *35*, 4116–4124.

(41) Lim, S. Y.; Hong, K. H.; Kim, D. I.; Kwon, H.; Kim, H. J. Tunable Heptamethine–Azo Dye Conjugate as an NIR Fluorescent Probe for the Selective Detection of Mitochondrial Glutathione over Cysteine and Homocysteine. *J. Am. Chem. Soc.* **2014**, *136*, 7018–7025.

(42) Sun, W.; Guo, S. G.; Hu, C.; Fan, J. L.; Peng, X. J. Recent Development of Chemosensors Based on Cyanine Platforms. *Chem*. *Rev*. **2016**, *116*, 7768–7817.

(43) Lou, Z.; Li, P.; Han, K. L. Redox-Responsive Fluorescent Probes with Different Design Strategies. *Acc*. *Chem*. *Res*. **2015**, *48*, 1358–1368.

(44) Chevalier, A.; Zhang, Y.; Khdour, O. M.; Kaye, J. B.; Hecht, S. M. Mitochondrial Nitroreductase Activity Enables Selective Imaging and Therapeutic Targeting. *J*. *Am*. *Chem*. *Soc*. **2016**, *138*, 12009–12012.

(45) Yin, J.; Kwon, Y. H.; Kim, D. B.; Lee, D. Y.; Kim, G.; Hu, Y.; Ryu, J. H.; Yoon, J. Y. Preparation of a Cyanine-Based Fluorescent Probe for Highly Selective Detection of Glutathione and Its Use in Living Cells and Tissues of Mice. *Nat*. *Protoc*. **2015**, *10*, 1742–1754.

(46) Han, C. M.; Yang, H. R.; Chen, M.; Su, Q. Q.; Feng, W.; Li, F. Y. Mitochondria-Targeted Near-Infrared Fluorescent Off–On Probe for Selective Detection of Cysteine in Living Cells and in Vivo. *ACS Appl*. *Mater*. *Interfaces* **2015**, *7*, 27968–27975.

(47) Xu, Z.; Xu, L. Fluorescent Probes for the Selective Detection of Chemical Species inside Mitochondria. *Chem*. *Commun*. **2016**, *52*, 1094–1119.

(48) Xu, W.; Zeng, Z. B.; Jiang, J. H.; Chang, Y. T.; Yuan, L. Discerning the Chemistry in Individual Organelles with Small-Molecule Fluorescent Probes. *Angew. Chem., Int. Ed.* **2016**, *55*, 13658–13699.

(49) Jiang, N.; Fan, J. L.; Xu, F.; Peng, X. J.; Mu, H. Y.; Wang, J. Y.; Xiong, X. Q. Ratiometric Fluorescence Imaging of Cellular Polarity: Decrease in Mitochondrial Polarity in Cancer Cells. *Angew*. *Chem*., *Int*. *Ed*. **2015**, *127*, 2540–2544.

(50) Rong, P. F.; Huang, P.; Liu, Z. G.; Lin, J.; Jin, A.; Ma, Y.; Liu, G.; Yu, L.; Zeng, W. B.; Wang, W.; Chen, X. Y. Protein-Based Photothermal Theranostics for Imaging-Guided Cancer Therapy. *Nanoscale* **2015**, *7*, 16330–16336.

(51) Zhang, C.; Zhou, L.; Zhang, J.; Fu, Y. Y.; Zhang, X. J.; Yu, C. S.; Sun, S. K.; Yan, X. P. Green and Facile Synthesis of a Theranostic Nanoprobe with Intrinsic Biosafety and Targeting Abilities. *Nanoscale* **2016,** *8*, 16204–16211.

(52) Zhou, B. J.; Li, Y. Z.; Niu, G. L.; Lan, M. H.; Jia, Q. Y.; Liang, Q. L. Near-Infrared Organic Dye-Based Nanoagent for the Photothermal Therapy of Cancer. *ACS Appl*. *Mater*. *Interfaces* **2016**, *8*, 29899–29905.

(53) Guo, M.; Huang, J.; Deng, Y. B.; Shen, H.; Ma, Y. F.; Zhang, M. X.; Zhu, A. J.; Li, Y. L.; Hui, H.; Wang, Y. Y.; Yang, X. L.; Zhang, Z. J.; Chen, H. B. pH-Responsive Cyanine-Grafted Graphene Oxide for Fluorescence Resonance Energy Transfer-Enhanced Photothermal Therapy. *Adv*. *Funct*. *Mater*. **2015**, *25*, 59–67.

(54) Yu, H. J.; Cui, Z. R.; Yu, P. C.; Guo, C. Y.; Feng, B.; Jiang, T. Y.; Wang, S. L.; Yin, Q.; Zhong, D. F.; Yang, X. L.; Zhang, Z. W.; Li, Y. P. pH- and NIR Light-Responsive Micelles with Hyperthermia-Triggered Tumor Penetration and Cytoplasm Drug Release to Reverse Doxorubicin Resistance in Breast Cancer. *Adv*. *Funct*. *Mater*. **2015**, *25*, 2489–2500.

(55) Zheng, M. B.; Yue, C. X.; Ma, Y. F.; Gong, P.; Zhao, P. F.; Zheng, C. F.; Sheng, Z. H.; Zhang, P. F.; Wang, Z. H.; Cai, L. T. Single-Step Assembly of DOX/ICG Loaded Lipid–Polymer Nanoparticles for Highly Effective Chemo-Photothermal Combination Therapy. A*CS Nano* **2013**, *7*, 2056–2067.

(56) Chen, Z.; Zhao, P. F.; Luo, Z. Y.; Zheng, M. B.; Tian, H.; Gong, P.; Gao, G. H.; Pan, H.; Liu, L. L.; Ma, A. Q.; Cui, H. D.; Ma, Y. F.; Cai, L. T. Cancer Cell Membrane–Biomimetic Nanoparticles for Homologous-Targeting Dual-Modal Imaging and Photothermal Therapy. *ACS Nano* **2016**, *10*, 10049–10057.

(57) Luo, S. L.; Yang, Z. Y.; Tan, X.; Wang, Y.; Zeng, Y. P.; Wang, Y.; Li, C. M.; Li, R.; Shi, C. M. Multifunctional Photosensitizer Grafted on Polyethylene Glycol and Polyethylenimine Dual-Functionalized Nanographene Oxide for Cancer-Targeted Near-Infrared Imaging and Synergistic Phototherapy. *ACS Appl*. *Mater*. *Interfaces* **2016**, *8*, 17176–17186.

(58) Zhang, Y. Y.; Ang, C. Y.; Li, M. H.; Tan, S. Y.; Qu, Q. Y.; Zhao, Y. L. Polymeric Prodrug Grafted Hollow Mesoporous Silica Nanoparticles Encapsulating Near-Infrared Absorbing Dye for Potent Combined Photothermal-Chemotherapy. *ACS Appl*. *Mater*. *Interfaces* **2016**, *8*, 6869–6879.

(59) Cheng, Y. H.; Cheng, H.; Jiang, C. X.; Qiu, X. F.; Wang, K. K.; Huan, W.; Yuan, A. H.; Wu, J. H.; Hu, Y. Q. Perfluorocarbon Nanoparticles Enhance Reactive Oxygen Levels and Tumour Growth Inhibition in Photodynamic Therapy. *Nat*. *Commun*. **2015**, *6*, 8785.

(60) Yuan, A. H.; Qiu, X. F.; Tang, X. L.; Liu, W.; Wu, J. H.; Hu, Y. Q. Self-Assembled PEG-IR-780-C13 Micelle as a Targeting, Safe and Highly-Effective Photothermal Agent for in Vivo Imaging and Cancer Therapy. *Biomaterials* **2015**, *51*, 184–193.

(61) Zhang, E. L.; Luo, S. L.; Tan, X.; Shi, C. M. Mechanistic Study of IR-780 Dye as a Potential Tumor Targeting and Drug Delivery Agent. *Biomaterials* **2014**, *35*, 771–778.

(62) An, X. N.; Zhu, A. J.; Luo, H. H.; Ke, H. T.; Chen, H. B.; Zhao, Y. L. Rational Design of Multi-Stimuli-Responsive Nanoparticles for Precise Cancer Therapy. *ACS Nano* **2016**, *10*, 5947–5958.

(63) Wang, J. X.; Liu, Y.; Ma, Y. C.; Sun, C. Y.; Tao, W.; Wang, Y. C.; Yang, X. Z.; Wang, J. NIR-Activated Supersensitive Drug Release Using Nanoparticles with a Flow Core. *Adv*. *Funct*. *Mater*. **2016**, *26*, 7516–7525.

(64) An, Q.; Liu, J.; Yu, M.; Wan, J. X.; Li, D.; Wang, C. C.; Chen, C. Y.; Guo, J. Multifunctional Magnetic Gd^{3+}-Based Coordination Polymer Nanoparticles: Combination of Magnetic Resonance and Multispectral Optoacoustic Detections for Tumor-Targeted Imaging in Vivo. *Small* **2015**, *11*, 5675–5686.

(65) Li, Y. L.; Deng, Y. B.; Tian, X.; Ke, H. T.; Guo, M.; Zhu, A. J.; Yang, T.; Guo, Z. Q.; Ge, Z. S.; Yang, X. L.; Chen, H. B. Multipronged Design of Light-Triggered Nanoparticles To Overcome Cisplatin Resistance for Efficient Ablation of Resistant Tumor. *ACS Nano* **2015**, *9*, 9626–9637.

(66) Li, W.; Zhang, H. B.; Guo, X. M.; Wang, Z. H.; Kong, F. F.; Luo, L. H.; Li, Q. P.; Zhu, C. Q.; Yang, J.; Lou, L.; Du, Y. Z.; You, J. Gold Nanospheres-Stabilized Indocyanine Green as a Synchronous Photodynamic–Photothermal Therapy Platform That Inhibits Tumor Growth and Metastasis. *ACS Appl*. *Mater*. *Interfaces* **2017**, *9*, 3354–3367.

(67) Liu, Y. Y.; Lu, Z. Z.; Mei, L.; Yu, Q. W.; Tai, X. W.; Wang, Y.; Shi, K. R.; Zhang, Z. R.; He, Q. Tandem Peptide Based on Structural Modification of Poly-Arginine for Enhancing Tumor Targeting Efficiency and Therapeutic Effect. *ACS Appl*. *Mater*. *Interfaces* **2017**, *9*, 2083–2092.

(68) Ren, H.; Liu, J. Q.; Su, F. H.; Ge, S. Z.; Yuan, A. H.; Dai, W. M.; Wu, J. H.; Hu, Y. Q. Relighting Photosensitizers by Synergistic Integration of Albumin and Perfluorocarbon for Enhanced Photodynamic Therapy. *ACS Appl*. *Mater*. *Interfaces* **2017**, *9*, 3463–3473.

(69) Gao, S.; Wang, G. H.; Qin, Z. N.; Wang, X. Y.; Zhao, G. Q.; Ma, Q. J.; Zhu, L. Oxygen-Generating Hybrid Nanoparticles to Enhance Fluorescent/Photoacoustic/Ultrasound Imaging Guided Tumor Photodynamic Therapy. *Biomaterials* **2017**, *112*, 324–335.

(70) Topete, A.; Alatorre-Meda, M.; Iglesias, P.; Villar-Alvarez, E. M.; Barbosa, S.; Costoya, J. A.; Taboada, P.; Mosquera, V. Fluorescent Drug-Loaded, Polymeric-Based, Branched Gold Nanoshells for Localized Multimodal Therapy and Imaging of Tumoral Cells. *ACS Nano* **2014**, *8*, 2725–2738.

(71) Sheng, Z. H.; Hu, D. H.; Zheng, M. B.; Zhao, P. F.; Liu, H. L.; Gao, D. Y.; Gong, P.; Gao, G. H.; Zhang, P. F.; Ma, Y. F.; Cai, L. T. Smart Human Serum Albumin-Indocyanine Green Nanoparticles Generated by Programmed Assembly for Dual-Modal Imaging-Guided Cancer Synergistic Phototherapy. *ACS Nano* **2014**, *8*, 12310–12322.

(72) Ocsoy, I.; Isiklan, N.; Cansiz, S.; Özdemir, N.; Tan, W. H. ICG-Conjugated Magnetic Graphene Oxide for Dual Photothermal and Photodynamic Therapy. *RSC Adv*. **2016**, *6*,

30285–30292.

(73) Chen, Q.; Wang, C.; Zhan, Z. X.; He, W. W.; Cheng, Z. P.; Li, Y. Y.; Liu, Z. Near-Infrared Dye Bound Albumin with Separated Imaging and Therapy Wavelength Channels for Imaging-Guided Photothermal Therapy. *Biomaterials* **2014**, *35*, 8206–8214.

(74) Gong, X. Y.; Yang, X. F.; Zhong, Y. G.; Chen, Y. H.; Li, Z. A Mitochondria-Targetable Near-Infrared Fluorescent Probe for Imaging Nitroxyl (HNO) in Living Cells. *Dyes Pigments* **2016**, 131, 24–32.

(75) Samanta, A.; Maiti, K. K.; Soh, K. S.; Liao, X. J.; Vendrell, M.; Dinish, U. S.; Yun, S. W.; Bhuvaneswari, R.; Kim, H.; Rautela, S.; Chung, J. H.; Olivo, M.; Chung, Y. J. Ultrasensitive Near-Infrared Raman Reporters for SERS-Based in Vivo Cancer Detection. *Angew*. *Chem*., *Int*. *Ed*. **2011**, *50*, 6089–6092.

(76) Peng, X. Z.; Chen, H. X.; Draney, D. R.; Volcheck, W.; Schutz-Geschwender, A.; Olive, D. M. A Nonfluorescent, Broad-Range Quencher Dye for Förster Resonance Energy Transfer Assays. *Anal*. *Biochem*. **2009**, *388*, 220–228.

(77) Zou, Q. L.; Abbas, M.; Zhao, L. Y.; Li, S. K.; Shen, G. Z.; Yan, X. H. Biological Photothermal Nanodots Based on Self-Assembly of Peptide–Porphyrin Conjugates for Antitumor Therapy. *J*. *Am*. *Chem*. *Soc*. **2017**, *139*, 1921–1927.

(78) Li, K. C.; Chu, H. C.; Lin, Y.; Tuan, H. Y.; Hu, Y. C. PEGylated Copper Nanowires as a Novel Photothermal Therapy Agent. *ACS Appl*. *Mater*. *Interfaces* **2016**, *8*, 12082–12090.

(79) Ma, N. N.; Jiang, Y. W.; Zhang, X. D.; Wu, H.; Myers, J. N.; Liu, P. D.; Jin, H. Z.; Gu, N.; He, N. Y.; Wu, F. G.; Chen, Z. Enhanced Radiosensitization of Gold Nanospikes via Hyperthermia in Combined Cancer Radiation and Photothermal Therapy. *ACS Appl*. *Mater*. *Interfaces* **2016**, *8*, 28480–28494.

(80) Jin, B.; Zhang, X.; Zheng, W.; Liu, X. J.; Zhou, J.; Zhang, N.; Wang, F. Y.; Shangguan, D. H. Dicyanomethylene-Functionalized Squaraine as a Highly Selective Probe for Parallel G-Quadruplexes. *Anal*. *Chem*. **2014**, *86*, 7063–7070.

(81) Yang, Q. F.; Xiang, J. F.; Yang, S.; Zhou, Q. J.; Li, Q.; Tang, Y. L.; Xu, G. Z. Verification of Specific G-Quadruplex Structure by Using a Novel Cyanine Dye Supramolecular Assembly: I. Recognizing Mixed G-Quadruplex in Human Telomeres. *Chem*. *Commun*. **2009**, 1103–1105.

(82) Cheng, L.; He, W. W.; Gong, H.; Wang, C.; Chen, Q.; Cheng, Z. P.; Liu, Z. PEGylated Micelle Nanoparticles Encapsulating a Non-Fluorescent Near-Infrared Organic Dye as a Safe and Highly-Effective Photothermal Agent for in Vivo Cancer Therapy. *Adv*. *Funct*. *Mater*. **2013**, *23*, 5893–5902.

(83) Zhang, G.; Sun, Y. M.; He, X. Q.; Zhang, W. J.; Tian, M. G.; Feng, R. Q.; Zhang, R. Y.; Li, X. C.; Guo, L. F.; Yu, X. Q.; Zhang, S. L. Red-Emitting Mitochondrial Probe with Ultrahigh Signal-to-Noise Ratio Enables High-Fidelity Fluorescent Images in Two-Photon Microscopy. *Anal*. *Chem*. **2015**, *87*, 12088–12095.

(84) Gui, C.; Zhao, E. G.; Kwok, R. T. K.; Leung, A. C. S.; Lam, J. W. Y.; Jiang, M. J.; Deng, H. Q.; Cai, Y. J.; Zhang, W. J.; Su, H. F.; Tang, B. Z. AIE-Active Theranostic System: Selective Staining and Killing of Cancer Cells. *Chem*. *Sci*. **2017**, *8*, 1822–1830.

(85) Lan, B. C. Mitochondrial Membrane Potential in Living Cells. *Annu*. *Rev*. *Cell Biol*. **1988**, *4*, 155–181.

(86) Nani, R. R.; Kelley, J. A.; Ivanic, J.; Schnermann, M. J. Reactive Species Involved in the Regioselective Photooxidation of Heptamethine Cyanines. *Chem*. *Sci*. **2015**, *6*, 6556–6563.

(87) Singh, S.; Aggarwal, A.; Bhupathiraju, N. V. D. K.; Arianna, G.; Tiwari, K.; Drain, C. M. Glycosylated Porphyrins, Phthalocyanines, and Other Porphyrinoids for Diagnostics and Therapeutics. *Chem*. *Rev*. **2015**, *115*, 10261–10306.

TOC Graphic

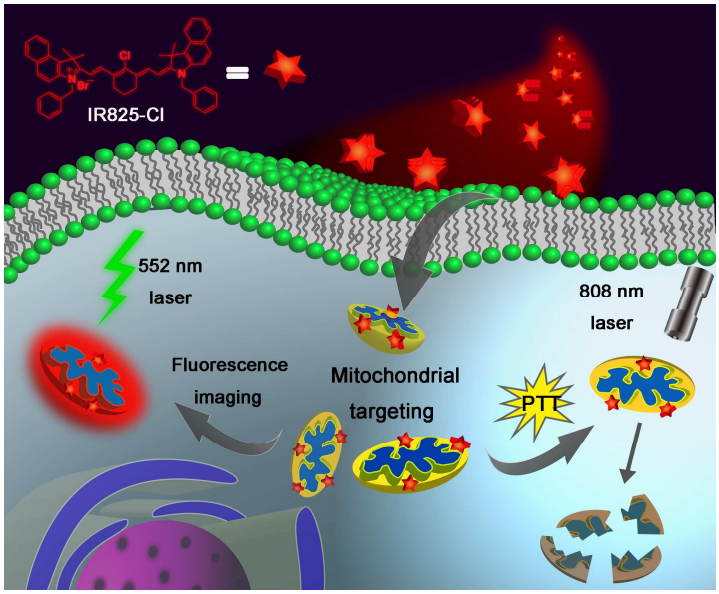
IR825-Cl
552 nm
laser
Fluorescence
imaging
Mitochondrial
targeting
PTT
808 nm
laser